Inorg. Chem. **2004**, *43*, 8072–8077

A Chiral Molecular Conductor: Synthesis, Structure, and Physical Properties of $[ET]_3[Sb_2(L\text{-tart})_2]\cdot CH_3CN$ (ET = Bis(ethylendithio)tetrathiafulvalene; L-tart = (2*R*,3*R*)-(+)-Tartrate)

Eugenio Coronado,*,† José R. Galán-Mascarós,*,† Carlos J. Gómez-García,† Ana Murcia-Martínez,† and Enric Canadell‡

Instituto de Ciencia Molecular, Universidad de Valencia, C/ Doctor Moliner 50, 46100 Burjassot, Spain, and Institut de Ciència de Materials de Barcelona (CSIC), Campus de la UAB, 08193—Bellaterra, Spain

Received June 8, 2004

The salt $[ET]_3[Sb_2(L\text{-tart})_2]\cdot CH_3CN$ (**1**) has been obtained by electrocrystallization of the organic donor bis(ethylendithio)-tetrathiafulvalene (ET or BEDT-TTF) in the presence of the chiral anionic complex $[Sb_2(L\text{-tart})_2]^{2-}$ (L-tart = (2*R*,3*R*)-(+)-tartrate). This salt crystallizes in the chiral space group $P2_12_12_1$ (a = 11.145(2) Å, b = 12.848(2) Å, c = 40.159(14) Å, V = 5750.4(14) Å^3, Z = 4) and is formed by alternating layers of the anions and of the organic radicals in a noncentrosymmetric α-type packing. This compound shows a room temperature electrical conductivity of $\sim$1 S·cm^{-1} and semiconducting behavior with an activation energy of $\sim$85 meV. Analysis of the magnetic susceptibility and band structure, however, suggests that this compound should be a narrow band gap semiconductor.

Introduction

The interest in molecular materials has grown extensively in recent years mostly due to the really unique approaches that they offer for different areas of materials research which are difficult to tackle through other perspective such as multifuctional,[1] nanostructured,[2] or biomedical materials.[3] With respect to multifuncionality, the molecular approach has been very successful, yielding new materials that combine in the solid state two or more physical properties of interest by combination of two or more molecular building blocks. This strategy has been particularly exploited in the case of materials combining electrical conductivity with a second property.

The so-called organic conductors based on tetrathiafulvalene, TTF, and derivatives[4] represent the most extended family of organic metals and superconductors and, therefore, have been subject of multiple studies. In addition to their electrical properties, their tendency to create segregated stacks in the radical salts with different types of anions have made them very useful building blocks for the design and construction of multifunctional molecular materials wherein the TTF network will give rise to conducting properties, while the functional anions will be responsible for the inclusion of a second physical property of interest in the solid. Paramagnetic complexes have been used for the preparation of organic semiconductors,[5] metals,[6] and even superconductors,[7] where delocalized electrons coexist with the localized electrons in the paramagnetic centers. Ferro-

* To whom correspondence should be addressed. E-mail: eugenio.coronado@uv.es (E.C.); jose.r.galan@uv.es (J.R.G.-M.).
† Universidad de Valencia.
‡ Institut de Ciència de Materials de Barcelona (CSIC).

(1) Coronado, E.; Forment-Aliaga, A.; Galán-Mascarós, J. R.; Giménez-Saiz, C.; Gómez-García, C. J.; Martínez-Ferrero, E.; Nuez, A.; Romero, F. M. *Solid State Sci.* **2003**, *5*, 917−924.
(2) Maruccio, G.; Cingolani, R.; Rinaldi, R. *J. Mater. Chem.* **2004**, *14*, 542−554.
(3) Reichert, D. E.; Lewis, J. S.; Anderson, C. J. *Coord. Chem. Rev.* **1999**, *184*, 3−66.
(4) Williams, J. M.; Ferraro, J. R.; Thorn, R. J.; Carlson, K. D.; Geiser, U.; Wang, H. H.; Kini, A. M.; Whangbo, M. H. In *Organic Superconductors (Including Fullerenes). Synthesis, Structure, Properties and Theory*; Grimes, R. N., Ed.; Prentice Hall: Englewood Cliffs, NJ, 1992.
(5) (a) Mallah, T.; Hollis, C.; Bott, S.; Kurmoo, M.; Day, P. *J. Chem. Soc., Dalton Trans.* **1990**, 859−865. (b) Clemente-León, M.; Coronado, E.; Galán-Mascarós, J. R.; Giménez-Saiz, C.; Gómez-García, C. J.; Ribera, E.; Vidal-Gancedo, J.; Rovira, C.; Canadell, E.; Laukhin, V. N. *Inorg. Chem.* **2001**, *40*, 3526−3533.
(6) (a) Mori, H.; Hirabayashi, I.; Tanaka, S.; Mori, T.; Manyama, Y. *Synth. Met.* **1995**, *70*, 789−790. (b) Coronado, E.; Falvello, L. R.; Galán-Mascarós, J. R.; Giménez-Saiz, C.; Gómez-García, C. J.; Laukhin, V. N.; Pérez-Benítez, A.; Rovira, C.; Veciana, J. *Adv. Mater.* **1997**, *9*, 984−987.

10.1021/ic049257e CCC: $27.50
Published on Web 11/02/2004

magnetic layers have been used for the preparation of the first ferromagnetic molecular metals.[8,9] Photochromic complexes such as nitroprusside have yielded photoactive conductors.[10] This very same approach can be extended to other anionic complexes, and one of the most attractive possibilities is that of chiral complexes or molecules. Chirality is an important property of matter, since it creates an anisotropy in the system that affects all macroscopic behavior of a material including, but not limited to, their optical properties.

Several chiral magnets have been developed on the basis of chiral molecular building blocks,[11−13] although the effect of the anisotropy on the magnetic properties is still unclear. For instance, in these chiral magnets no evidence of magnetochiral dichroism has been reported so far, as it was described for chiral paramagnetic systems in solution.[14] The effect that chirality could have on the electrical conductivity has not been studied in detail yet. Several known conductors are chiral, though, either because they crystallize in a chiral space group without any further synthetic control such as tellurium or β-manganese,[15] or because chiral precursors have been used for their preparation, such as in chiral conducting polymers,[16] DNA molecules,[17] and organic conductors based on chiral TTF derivatives.[18] Rikken has predicted that chiral electrical conductors should show electrical magneto-chiral anisotropy.[19] This effect should be observed in the magneto-transport properties of the material. The electrical resistance is expected to have different values upon reversal of both the direction of the current, and that of the external magnetic field. The electrical magneto-chiral anisotropies observed thus far are quite small, but it has been pointed out that they may be interesting in spintronics since in chiral conductors electrical resistance depends not only on the magnitude of spin polarization, but also on its direction. These expectations justify the design and investigation of this class of dual-function materials. Dealing with the molecular conductors, the chirality of the two-network solid can be deliberately introduced by using a chiral anion complex as charge-compensating counterion. Herein we report the synthesis, structure, and physical characterization of a novel chiral conductor $[ET]_3[Sb_2(L\text{-tart})_2]\cdot CH_3CN$ (**1**), from the building blocks bis(ethylendithio)tetrathiafulvalene (BEDT-TTF or ET) and the L-tartrate (L-tart) based chiral dimer $[Sb_2(L\text{-tart})_2]^{2-}$ (Figure 1).

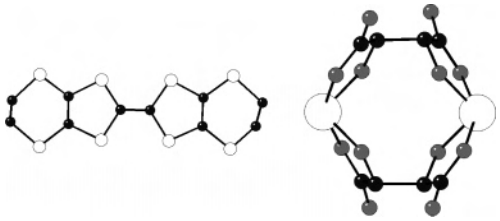

Figure 1. BEDT-TTF and $[Sb_2(L\text{-tart})_2]$.

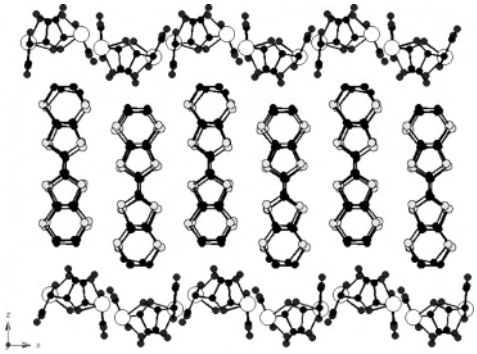

Figure 2. View of the alternating layers in the $[ET]_3[Sb_2(L\text{-tart})_2]\cdot CH_3CN$ (**1**) salt.

Crystal Structure

The $[ET]_3[Sb_2(L\text{-tart})_2]\cdot CH_3CN$ (**1**) salt was prepared by electrochemical oxidation of ET in the presence of $[Sb_2(L\text{-tart})_2]^{2-}$ as dark brown, long, needlelike crystals. This compound crystallizes in the chiral orthorhombic space group $P2_12_12_1$, as imposed by the chirality of the anions. It is formed by alternating layers of anions and of ET radical cations (Figure 2). The latter arrange following a typical packing of the so-called α-phases (Figure 4), with three different types of ET molecules, A, B, and C. These molecules stack forming chains along the *b*-axis following

(7) (a) Kurmoo, M.; Graham, A. W.; Day, P.; Coles, S. J.; Hursthouse, M. B.; Caulfield, J. M.; Singleton, J.; Ducasse, L.; Guionneau, P. *J. Am. Chem. Soc.* **1995**, *117*, 12209−12217. (b) Kobayashi, H.; Sato, A.; Arai, E.; Akutsu, H.; Kobayashi, A.; Cassoux, P. *J. Am. Chem. Soc.* **1997**, *119*, 12392−12393.

(8) Coronado, E.; Galán-Mascarós, J. R.; Gómez-García, C. J.; Laukhin, V. *Nature* **2000**, *408*, 447−449.

(9) (a) Alberola, A.; Coronado, E.; Galán-Mascarós, J. R.; Giménez-Saiz, C.; Gómez-García, C. J. *J. Am. Chem. Soc.* **2003**, *125*, 10774−10775. (b) Alberola, A.; Coronado, E.; Galán-Mascarós, J. R.; Giménez-Saiz, C.; Gómez-García, C. J.; Romero, F. M. *Synth. Met.* **2003**, *133*−*134*, 509−513. (c) Alberola, A.; Coronado, E.;. Galán-Mascarós, J. R.; Giménez-Saiz, C.; Gómez-García, C. J.; Martínez-Ferrero, E.; Murcia-Martínez, A. *Synth. Met.* **2003**, *135*−*136*, 687−689.

(10) (a) Clemente-León, M.; Coronado, E.; Galán-Mascarós, J. R.; Gómez-García, C. J.; Canadell, E. *Inorg. Chem.* **2000**, *39*, 5394−5397. (b) Clemente-León, M.; Coronado, E.; Galán-Mascarós, J. R.; Giménez-Saiz, C.; Gómez-García, C. J.; Ribera, E.; Vidal-Gancedo, J.; Rovira, C.; Canadell, E.; Laukhin, V. *Inorg. Chem.* **2001**, *40*, 3526−3522.

(11) (a) Coronado, E.; Gómez-García, C. J.; Nuez, A.; Romero, F. M.; Rusanov, E.; Stoeckli-Evans, H. *Inorg. Chem.* **2002**, *41*, 4615−4617. (b) Inoue, K.; Imai, H.; Ghalsasi, P. S.; Kikuchi, K.; Ohba, M.; Okawa, H.; Yakhmi, J. V. *Angew. Chem., Int. Ed.* **2001**, *40*, 4242−424.

(12) (a) Coronado, E.; Galán-Mascarós, J. R.; Gómez-García, C. J.; Martínez-Agudo, J. M. *Inorg. Chem.* **2001**, *40*, 113−120. (b) Andres, R.; Brissard, M.; Gruselle, M.; Train, C.; Vaisserman, J.; Malezieux, B.; Jamet, J. P.; Verdaguer, M. *Inorg. Chem.* **2001**, *40*, 4633−4640.

(13) Minguet, M.; Luneau, D.; Lhotel, E.; Villar, V.; Paulsen, C.; Amabilino, D. B.; Veciana, J. *Angew. Chem., Int. Ed.* **2002**, *41*, 586−588.

(14) Rikken, G. L. J. A.; Raupach, E. *Nature* **1997**, *390*, 493−494.

(15) *CRC Handbook of Chemistry and Physics*, 77th ed.; Lide, D. R., Ed.; CRC Press: Boca Raton, FL, 1997.

(16) (a) Akagi, K.; Piao, G.; Kaneko, S.; Sakamaki, K.; Shirakawa, H.; Kyotani, M. *Science* **1998**, *282*, 1683−1686. (b) Tigelaar, D. M.; Lee, W.; Bates, K. A.; Saprigin, A.; Prigodin, V. N.; Cao, X.; Nafie, L. A.; Plarz, M. S.; Epstein, A. J. *Chem. Mater.* **2002**, *14*, 1430−1438.

(17) (a) Fink, H.-W.; Schönenberger, C. *Nature* **1999**, *398*, 407−410. (b) Porath, D.; Bezryadin, A.; de Vries, S.; Dekker, C. *Nature* **2000**, *403*, 635−638.

(18) (a) Zambounis, J. S.; Pfeiffer, J.; Papavassiliou, G. C.; Lagouvardos, D. J.; Terzis, A.; Delhàes, C. P.; Ducasse, L.; Fortune, N. A.; Murata, K. *Solid State Commun.* **1995**, *95*, 211−215. (b) Murata, K.; Shirakawa, N.; Yoshino, H.; Tsubaki, Y.; Papavassiliou, G. C.; Terzis, A.; Zambounis, J. S. *Synth. Met.* **1997**, *86*, 2021−2022. (c) Olejniczak, I.; Jones, B. R.; Zhu, Z.; Dong, J.; Musfeld, J. L.; Schlueter, J. A.; Morales, E.; Geiser, U.; Nixon, P. G.; Winter, R. W.; Gard, G. L. *Chem. Mater.* **1999**, *11*, 3160−3165.

(19) Rikken, G. L. J. A.; Fölling, J.; Wyder, P. *Phys. Rev. Lett.* **2001**, *87*, 236602.

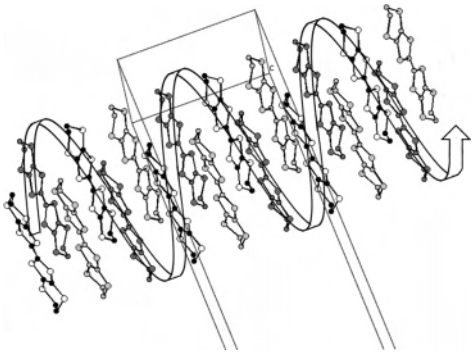

Figure 3. View of the helicoidal structure of the organic layer in the $[ET]_3[Sb_2(L\text{-tart})_2]\cdot CH_3CN$ (**1**) salt along the *b*-axis by donor molecules A (black and yellow), B (green), and C (blue).

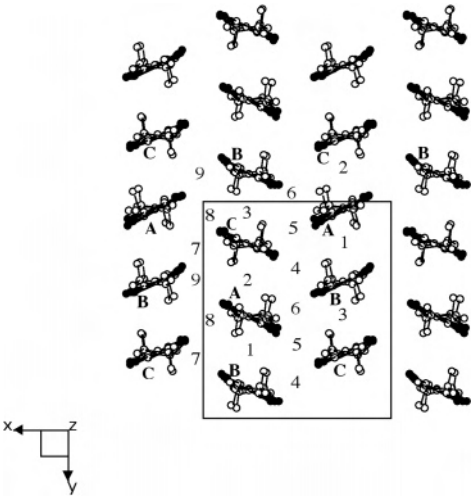

Figure 4. Top view of the organic layers in the $[ET]_3[Sb_2(L\text{-tart})_2]\cdot CH_3CN$ (**1**) salt showing the α-type packing mode of the organic radicals and the nine different types of donor−donor interactions.

an ...ABCABC... sequence, with A−B, B−C, and A−C intrachain distances very similar to each other (closest S−S contacts being S8−S15 = 4.111(5) Å, S16−S26 = 4.127(5) Å, and S5−S28 = 4.193(5) Å) resulting in a quite regular chain. But this structure has a clear 2D character as the closer contacts are side contacts between chains. The interchain contacts (S7−S28 = 3.472(5) Å; S15−S27 = 3.468(5) Å) are much shorter than the sum of van der Waals radii (3.6 Å), indicating that there are some bidimensional interactions. The molecules within the layers are related through 2-fold screw axis parallel to the *a*- and *b*-axis, creating helicoidal substructures half a unit cell wide with a period of one unit cell (Figure 3).

From the bonding distances, the charge residing in each ET molecule can be estimated, taking into account that there are two positive charges for three ET molecules. Two of them appear to be almost completely oxidized with a charge close to +1(A and B) while the third one (C) appears to be almost neutral (∼+0.2). This result is surprising since the structure of the chains is quite regular, although the charge is apparently not equally distributed. The typical crystallographic disorder usually found for the terminal ethylenic groups of the ET salts due to the two possible conformations of the $-CH_2-$ groups (up or down the mean plane of the

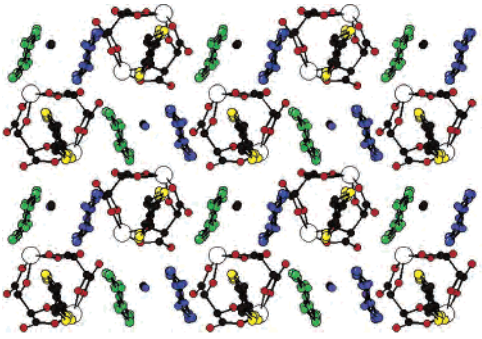

Figure 5. Top view of two adjacent layers in the $[ET]_3[Sb_2(L\text{-tart})_2]\cdot CH_3CN$ (**1**) salt showing the different disposition with respect to the anions of donor molecules A (black and yellow), B (green), and C (blue).

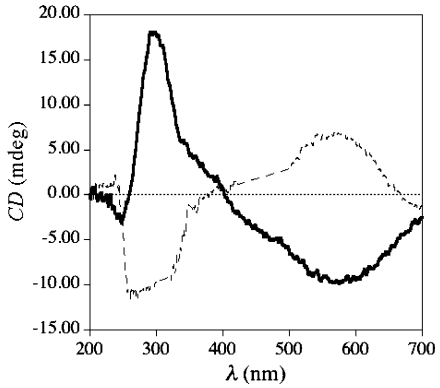

Figure 6. Circular dichroism spectra for $[ET]_3[Sb_2(L\text{-tart})_2]\cdot CH_3CN$ (**1**, —), and $[ET]_3[Sb_2(D\text{-tart})_2]\cdot CH_3CN$ (**2**, - - -).

ET molecules) appears here only for one of the ethylenic groups of molecule A.

The inorganic layer shows a pseudohexagonal arrangement of the $[Sb_2(L\text{-tart})_2]^{2-}$ dimers, with solvent molecules (acetonitrile) occupying the holes left in the structure by the anions. The nitrile groups of the solvent molecules point alternatively up and down.

The two layers show several hydrogen bonding contacts between the ethylenic groups of the ET molecules and the carboxylate groups of the anions. The two layers are disposed in such a way that molecule A is forming a sandwich between two $[Sb_2(L\text{-tart})_2]^{2-}$ anions with the shortest H bonding interactions (O2−H91 = 2.13(2) Å, and O2−H94 = 2.24(2) Å) on one side, and slightly longer to the other side (O3−H82 = 2.37(2) Å, Figure 5). It is worth mentioning that the strongest hydrogen bonding appears between the anions and the ethylenic group that appears crystallographically disordered, although it is not well understood why this happens. Molecules B and C are not those directly related to the anions although they also show short H contacts, even when according to the charge distribution molecule C should be close to neutrality (shortest contacts for B and C: O6−H192 = 2.40(2) Å, and O7−H302 = 2.25 Å, respectively).

Physical Properties

The circular dichroism absorption spectra of **1** (Figure 6) show clear CD activity with strong Cotton effects. There is CD activity in almost all the range of the UV−vis region, showing one continuous very broad band of negative sign

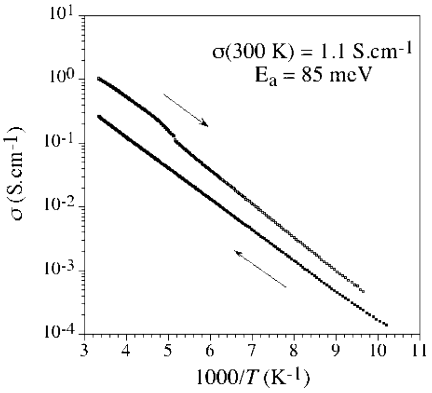

Figure 7. Thermal behavior of the electrical conductivity for $[ET]_3[Sb_2(L\text{-tart})_2]\cdot CH_3CN$ (**1**).

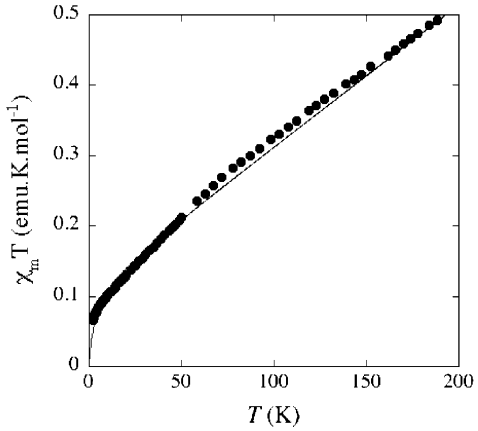

Figure 8. Thermal dependence of the magnetic susceptibility as the χT product for $[ET]_3[Sb_2(L\text{-tart})_2]\cdot CH_3CN$ (**1**). The solid line shows the best fit: $\chi_m T = [\chi_{TIP}\ T + C]$.

with its maximum around 570 nm and one more intense band of positive sign around 290 nm. Since the anions only show absorption in the UV range, below 240 nm in the solid state (see Supporting Information), the observed CD activity must be assigned to the organic part and therefore related to the conducting lattice. This confirms that the overall chirality of the crystal also affects the organic radicals, even if the individual molecules are nonchiral. The analogous salt $[ET]_3[Sb_2(D\text{-tart})_2]\cdot CH_3CN$ (**2**) has also been obtained, and it shows analogous CD activity but with the opposite sign, as expected.

Transport properties measured on single crystals with the four contacts method in the range 2−300 K show a typical semiconducting behavior (Figure 7), with a room temperature conductivity of 1 $S\cdot cm^{-1}$. From the slope of the ln ρ versus $1/T$ graph, an activation energy of 85 meV is found for these materials. This situation seems to agree with the crystal structure analysis which suggests some structurally induced charge localization in the system, but at the same time close intermolecular contacts in the organic layer.

The magnetic behavior (Figure 8), according to the magnetic measurements performed on polycrystalline samples in the same temperature range, is dominated by a temperature independent paramagnetism (2×10^{-3} emu mol^{-1}). This χ_{TIP} is too high to be exclusively attributed to the $[Sb_2(L\text{-tart})_2]^{2-}$ anion (Van Vleck's TIP estimated as $\sim 1 \times 10^{-3}$ for the potassium salt); thus, there should include a contribution from

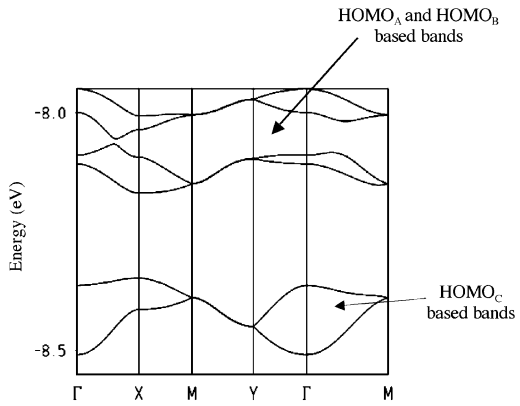

Figure 9. Calculated band structure for a donor layer of $[ET]_3[Sb_2(L\text{-tart})_2]\cdot CH_3CN$ (**1**) where $\Gamma = (0, 0)$, $X = (a^*/2, 0)$, $Y = (0, b^*/2)$, and $M = (a^*/2, b^*/2)$.

the conducting electrons in the organic lattice (Pauli paramagnetism, although this may contrast with the activated conductivity, see discussion below). There is also an additional paramagnetic contribution ($C = 0.13$ emu K mol^{-1}). In most radical salts, such a contribution is assigned to the presence of defects in the structure, but in this case the contribution is quite high (about $^1/_3$ of an electron every 3 ET molecules), and in addition to crystallographic defects, it is also probably related to the presence of some kind of charge localization in the system whose origin is as yet not clear. Magnetoresistance measurements were also performed in the search for evidence of the predicted electrical magneto-chiral anisotropy, but the resistance barely changes under applied external magnetic fields at high temperatures, and at low temperatures the resistance is too high.

Band Structure Calculations

In order to have some insight into the relationship between the crystal structure and transport properties of $[ET]_3[Sb_2(L\text{-tart})_2]\cdot CH_3CN$ (**1**), we have carried out tight binding band structure calculations for the donor layers of this material. The calculated band structure near the Fermi level is shown in Figure 9. There are six bands mainly built from the donors HOMO because the repeat unit of the layer contains six donor molecules. The bands occur as three sets of double degenerate bands along the $M-Y$ direction because of the existence of nonsymmorphic symmetry elements parallel to the b-direction (i.e., the 2_1 screw axes). Analysis of the wave vectors clearly shows that the lower lying pair of bands is mostly made of the HOMO of donors C whereas the set of four upper bands results from the mixing of the HOMOs of donors A and B. Because of the stoichiometry, there must be four holes in the bands of Figure 9. Consequently, the $HOMO_C$ based bands are full whereas those resulting from the mixing of $HOMO_A$ and $HOMO_B$ are only half-filled. These results confirm that donor C can be formally considered as neutral whereas donors A and B can be considered as ET^+. As shown in Figure 4, the donor layers are built from parallel stacks along the b-direction condensed in a typical α mode. There are three different donor−donor interactions along the stacks and six different donor−donor interstack interactions. As noted above, the interstack inter-

actions are associated with considerably shorter S−S contacts so that it is tempting to associate the 2D nature of the bands to these interactions. However, this would not be completely correct because the strength of the interaction between two HOMOs is proportional to the square of their overlap but inversely proportional to their energy difference. In molecular conductors, the overlaps are always relatively weak so that not very large HOMO energy differences can strongly reduce the effective HOMO−HOMO interaction. This is what occurs here because of the different formal charge between C (ET^0) and A/B (ET^+) donors which leads to a large $HOMO_C-HOMO_{A/B}$ energy difference (∼0.3 eV). Simply speaking, it should be expected that interactions implicating C should be quite weak. This is indeed the case since the two interstack HOMO−HOMO interactions associated with A−B interactions are the only ones which have sizable values. The intrastack A−B interaction although smaller is also non-negligible. As can be seen in Figure 4, every (A−B) pair directly sees four other (A−B) units leading thus to a 2D lattice of interactions. There are the two interstack and one intrastack A−B interactions which are the main contributors to the bandwidth of the upper four bands and, thus, to the conductivity of the material (see below), despite the fact that the shortest interstack contacts implicate donor C. Of course, interactions through C are not nil (otherwise the lower two bands would be dispersionless; but note that a large part of their dispersion results from interaction with slightly lower bands not shown in the figure) but are considerably smaller than expected and have a secondary role in the upper four bands region.

The important point in Figure 9 is the existence of a small band gap between the second and third upper bands as a consequence of an avoided crossing between the bands. We have carefully examined the behavior of the two bands inside the Brillouin zone to be sure that because of the dispersion along other directions, the two bands do not really overlap. It turns out that the band gap is real and amounts to 11 meV. Since there must be four holes in these bands, this result suggests that $[ET]_3[Sb_2(L\text{-tart})_2]\cdot CH_3CN$ may be a narrow band gap semiconductor. However, we should bear in mind that because of the weakness of many of the HOMO−HOMO interactions as a result of the charge separation, the bandwidths associated with the upper bands are only moderate raising the possibility of an electronic localization. In that case, the conductivity would also be activated. However, in such a case there would be four unpaired electrons per repeat unit (i.e., two per formula unit), something which is not supported by the magnetic measurements. In contrast, the existence of a very narrow band gap can naturally explain the above-mentioned contribution of the organic lattice to the TIP. The exact value of the narrow band gap is something which is beyond the capabilities of a semiempirical method like the present one. We note that the very narrow band gap, however, is stable to reasonable changes in the transfer integrals while keeping the charge separation in the donor lattice. Thus, we are confident that the band structure of Figure 9 must correctly describe the electronic structure of the donor lattice in **1**. In particular, there is no way to open a band gap consistent with the above resistivity measurements without completely altering the relative magnitude of the different transfer integrals or the observed charge separation in a way which would be inconsistent with the crystal structure. These observations suggest that the crystal and electronic structure studies are consistent with the magnetic measurements but not with the resistivity ones. Thus, the most plausible explanation points to the experimental presence of an unclear effect that dominates the resistivity measurements and masks the real conductivity of the material.

Finally, let us note that the crossing between the second and third bands is not symmetry allowed along the $\Gamma-X$ direction or inside the Brillouin zone associated with this donor lattice. Consequently, it is not likely that some kind of band overlap leading to metallic behavior can be realized as far as the symmetry group is kept and charge separation occurs. If the avoided crossing is disregarded, the four upper bands in Figure 9 can be seen as the superposition of two pairs of bands. As the A−B intrastack interaction increases, these two pairs of bands separate and eventually will not superpose anymore leading to larger band gaps. Thus, inducing an A−B dimerization in the stacks most likely would even decrease the conductivity. It is not clear what would be the effect of suppressing the charge localization while keeping the symmetry since the structural details can either be in favor or against the existence of a band overlap at the Fermi level. However, this may be the more tempting alternative for realizing the metallic state while keeping the structure.

Conclusion

Chirality is a property of molecules, and thus, the use of chiral molecules as building blocks constitutes a convenient strategy for the preparation of molecular materials that add chirality to a second property, such as magnetism or electrical conductivity. Some serendipitously obtained chiral conductors are known, but obviously a more general approach is desired. In this regard, the molecular conductors based on organic radicals offer many advantages, as shown, and due to their hybrid nature two different possibilities can be explored. Others have developed the synthesis of chiral counterparts of TTF derivatives in the search for molecular conductors, although this route is very costly synthetically, which limits the use of such an approach for general and exhaustive studies. Here, we have presented an alternative route, that of combining inorganic chiral counterions, readily available, stable, and easy to prepare, with symmetrical organic molecules. In particular, the salt **1** was prepared from the well-known achiral organic donor ET using as counterion a chiral dianion. The result is a chiral semiconductor, although the real extent of the conductivity is not yet clear. Analysis of the magnetic susceptibility and band structure suggests that the material should be a narrow band gap semiconductor. Work is in progress in order to fully understand the conductivity process in this material. Whatever the result will be, it is easy to envision how this convenient strategy can now be extended to many other

combinations of TTF derivatives with different inorganic chiral anions, where even additional functionalities could be added, including magnetism. Tartrate-based paramagnetic analogues have successfully been used in our lab to prepare magnetic chiral molecular conductors, increasing the multifunctionality in such systems, and these results will be reported soon.

Experimental Section

Synthesis. All reagents and solvents used were of commercially available grade. For $K_2[Sb_2(L\text{-tart})_2]$, potassium hydrogen tartrate (82 g) was dissolved in 400 mL of H_2O. Antimony(III) oxide (57.5 g) was added slowly with stirring. The solution was heated for 2 h at 80−90 °C, then allowed to cool to toom temperature, and then filtered. Ethanol was added to crash out the product, which was isolated by filtration and allowed to dry overnight. $[ET]_3[Sb_2(L\text{-tart})_2]\cdot CH_3CN$ (**1**) and $[ET]_3[Sb_2(D\text{-tart})_2]\cdot CH_3CN$ (**2**) were obtained on a platinum wire electrode by anodic oxidation of the organic donor ET (10 mg) in a U-shaped electrocrystallization cell in the presence of the salt $K_2[Sb_2(L\text{-tart})_2]$ (66 mg) or $K_2[Sb_2(D\text{-tart})_2]$, solubilized with 18-crown-6 ether (52 mg). A mixture of acetonitrile and benzonitrile (2:1) was used as solvent with a total volume of 20 mL. Stable, brown, elongated plates were obtained after 1 week applying a constant current intensity of 0.5 μA.

X-ray Crystallography. A dark brown, elongated, platelike single crystal of **1** ($0.5 \times 0.2 \times 0.05$ mm^3) was fixed on a glass fiber with epoxy glue and mounted on a KappaCCD diffractometer equipped with a graphite-monochromated Mo Kα radiation ($\lambda = 0.71069$). The frames were integrated and the data corrected for absorption using the KappaCCD software package (MAXUS). The structure was solved by direct methods using the SIR97 program,[20] and refined on F^2 with the SHELXL-97 program.[21] A total of 8637 unique reflections were collected. The crystal system was determine to be orthorhombic, $P2_12_12_1$. All non-hydrogen atoms were located after successive Fourier difference maps, and also those H atoms bound to the C atoms in the tartrate ligands, that were then refined with a restraint to maintain similar bonding lengths. The rest of the H atoms were placed in calculated positions with their thermal parameters fixed to be 20% larger than those of the atoms to which they are bound, and 50% in the case of H atoms from the methyl group in solvent to the solvent molecule. One of the ethylenic groups from an ET molecule appears crystallographically disordered over two different positions and was refined with occupancy factor $^1/_2$ for the two different conformations. All non-hydrogen atoms were refined anisotropically. Crystal, data collection, and refinement parameters are summarized in Table 1.

Physical Measurements. Magnetic measurements were carried out with a Quantum Design (SQUID) magnetometer MPMS-XL-5 with an applied field of 1000 G (0.1 T) in the 2−300 K temperature range. Data were corrected for the diamagnetic contributions calculated using the Pascal constants. Electrical conductivity measurements were performed with a Quantum Design PPMS using a typical four probe setup in the 2−300 temperature range with a sensitivity limit of 0.01 μA and 1 mV. Contacts to the crystals were made by platinum wires (20 μm diameter) attached by graphite paste to the samples. With the same setup, magnetoresistance and electrical magnetochiral anisotropy were explored by measuring dc electrical conductivity in the presence of a dc magnetic field from −9 up to 9 T. Circular dichroism absorption spectra were performed on KBr pressed pellets and recorded with a Jasco J810 spectropolarymeter.

Table 1. Main Structural Parameters and Crystallographic Data for the Salt $[ET]_3[Sb_2(L\text{-tart})_2]\cdot CH_3CN$ (**1**)

formula	$C_{40}H_{31}NO_{12}S_{24}Sb_2$
M_w	1730.60
space group	$P2_12_12_1$
a (Å)	11.145(2)
b (Å)	12.848(2)
c (Å)	40.159(3)
V (Å^3)	5750.4(14)
Z	4
T (K)	293(2)
λ (Å)	0.71069
ρ_{calc} (g/cm^3)	1.999
μ (mm^{-1})	1.871
R1[a]	0.0400
wR2	0.0736

[a] $R1 = \sum(F_o - F_c)/\sum(F_o)$. $wR2 = [\sum[w(F_o^2 - F_c^2)^2]/\sum[w(F_o^2)^2]]^{1/2}$; $w = 1/[\sigma^2(F_o^2) + (0.0422P)^2]$ where $P = (F_o^2 + 2F_c^2)/3$.

Band Structure Calculations. The tight-binding band structure calculations were based upon the effective one-electron Hamiltonian of the extended Hückel method.[22] The off-diagonal matrix elements of the Hamiltonian were calculated according to the modified Wolfsberg−Helmholz formula.[23] All valence electrons were explicitly taken into account in the calculations, and the basis set consisted of double-ζ Slater-type orbitals for C and S and single-ζ Slater-type orbitals for H. The exponents, contraction coefficients, and atomic parameters for C, S, and H were taken from previous work.[24]

Acknowledgment. This work was supported by the Ministerio de Ciencia y Tecnología (Projects MAT2001-3507-C02-01 and BQU2002-01091), the DGI-Spain (Project BFM2003-03372-C03-01.), the Generalitat de Catalunya (Project 2001 SGR 333), and the Generalitat Valenciana (GV04A/77). A.M.-M. thanks the Ministerio de Educación, Cultura y Deporte, for a predoctoral fellowship.

Supporting Information Available: X-ray CIF file for $[ET]_3[Sb_2(L\text{-tart})_2]\cdot CH_3CN$ (**1**) which was also deposited with the Cambridge Crystallographic Data Center, CCDC-253081. UV−vis spectra for $K_2[Sb_2(L\text{-tart})_2]$ and $[ET]_3[Sb_2(L\text{-tart})_2]\cdot CH_3CN$ (**1**) measured on pressed pellets and recorded with a Shimadzu UV-2401PC spectrophotometer. This material is available free of charge via the Internet at http://pubs.acs.org.

IC049257E

(20) SIR97: Altomare, A.; Burla, M. C.; Camali, M.; Cascarano, G. L.; Giacovazzo, C.; Guagliardi, A.; Moliterni, A. G.; Polidori, G.; Spagna, R. *J. Appl. Crystallogr.* **1999**, *32*, 115−119.

(21) Sheldrick, G. M. *SHELXL-97*; University of Göttingen: Göttingen, Germany, 1997.

(22) Whangbo, M.-H.; Hoffmann, R. *J. Am. Chem. Soc.* **1978**, *100*, 6093−6098.

(23) Ammeter, J.; Bürgi, H.-B.; Thibeault, J.; Hoffmann, R. *J. Am. Chem. Soc.* **1978**, *100*, 3686−3692.

(24) Pénicaud, A.; Bounekeur, K.; Batail, P.; Canadell, E.; Auban-Senzier, P.; Jérome, J. *J. Am. Chem. Soc.* **1993**, *115*, 4101−4112.